18th International Conference on the Application of Computer
Science and Mathematics in Architecture and Civil Engineering
K. Gürlebeck and C. Könke (eds.)
Weimar, Germany, 07–09 July 2009

NODALLY INTEGRATED FINITE ELEMENTS

Sebastian Wolff*

**Center of Mechanics and Structural Dynamics*
at Vienna University of Technology, Karlsplatz 13/E2063, 1040 Wien, Austria.
E-mail: sw@allmech.tuwien.ac.at

Keywords: finite element method, integration methods, nodal integration, stabilization.

Abstract.

Nodal integration of finite elements has been investigated recently. Compared with full integration it shows better convergence when applied to incompressible media, allows easier remeshing and highly reduces the number of material evaluation points thus improving efficiency. Furthermore, understanding it may help to create new integration schemes in meshless methods as well.

The new integration technique requires a nodally averaged deformation gradient. For the tetrahedral element it is possible to formulate a nodal strain which passes the patch test. On the downside, it introduces non-physical low energy modes. Most of these "spurious modes" are local deformation maps of neighbouring elements.

Present stabilization schemes rely on adding a stabilizing potential to the strain energy. The stabilization is discussed within this article. Its drawbacks are easily identified within numerical experiments: Nonlinear material laws are not well represented. Plastic strains may often be underestimated. Geometrically nonlinear stabilization greatly reduces computational efficiency.

The article reinterpretes nodal integration in terms of imposing a nonconforming C0-continuous strain field on the structure. By doing so, the origins of the spurious modes are discussed and two methods are presented that solve this problem. First, a geometric constraint is formulated and solved using a mixed formulation of Hu-Washizu type. This assumption leads to a consistent representation of the strain energy while eliminating spurious modes. The solution is exact, but only of theoretical interest since it produces global support. Second, an integration scheme is presented that approximates the stabilization criterion. The latter leads to a highly efficient scheme. It can even be extended to other finite element types such as hexahedrals.

Numerical efficiency, convergence behaviour and stability of the new method is validated using linear tetrahedral and hexahedral elements.

1 INTRODUCTION

Nodal integration (short NI) originates from the class of meshfree methods. Using smooth shape functions nodal strain measures are naturally given and can be used for a NI rule. However, it suffers from spurious zero energy modes. The first nodally integrated approach in FEM is found in [5, 3] who integrated a tetrahedral element nodally. Earlier works were interested in reducing volumetric locking by applying nodally averaged pressure fields or averaged determinants of the deformation gradient, [2, 4] (a kind of selective integration mainly due to the shortcomings of pure NI). In [5], the deformation gradient was averaged at the nodes according to the relative volume of the surrounding elements. The authors found the new elements to be very efficient, but they already observed nonphysical low-energy modes, though they regarded these effects as little important since they appeared in a very limited number of usecases.

Another related approach is the smoothed finite element method, see eg. [8]. Herein, the integration domain of each finite element is subdivided into smoothing cells. For each cell, a constant smoothed strain tensor is computed. The smoothing cells around a node can be used to compute a nodal strain tensor suitable for NI. In case of a single smoothing cell per element, certain element types like hexahedrals tend to spurious zero-energy modes. The authors do not report any instabilities, but for a single smoothing cell per element their method resembles the nodally averaged tetrahedral of [5].

[6] derives an assumed strain method using the method of weighted residuals. The approach consistently extends to tetrahedral and hexahedral finite elements of linear and quadratic shape functions. Again, for linear tetrahedral elements it corresponds to the method of [5]. In [10], the approach of [6] is discussed in detail. Extensions to higher order hexahedrals are presented and the appearence of spurious modes eliminated using an artificial potential function.

Stabilization, that is the elimination of spurious modes, concerned several authors. In [1] the matter of singular modes is addressed by adding an artificial potential function to the strain energy that penalizes the norm of the pointwise stress residual being integrated over the volume covered by the described material. The pointwise stress residual is measured as the error of the strong equilibrium conditions. [5] suggested to stabilize the elements by using information on the deformation gradient from the last time step in explicit simulations. The stabilization of spurious modes was discussed in detail in [11]. They suggested a stabilization method that adds an artificial energy to the strain energy, similar to [1]. The new aspect of their contribution was that the modified tetrahedral elements exactly behave like linear elastic finite elements with standard Gaussian quadrature for small strains. This is done by penalizing the difference of the averaged nodal strain and the natural strain. A norm of this difference can be obtained by assembling an energy using a constant material tensor. In [9] this stabilization scheme was generalized and applied to NI of meshfree methods.

2 ASSUMED DEFORMATION GRADIENT

The NI scheme becomes computationally efficient, if one can provide a single strain measure per node in order to evaluate the nodal stress. Since the shape function gradients are discontinuous across the finite element boundaries, one has to apply some averaging scheme, i.e.

$$F_{A\alpha\beta} = \frac{\sum_{m\in A}\sum_{e\in m} V_A^e F_{A\alpha\beta}^e}{V_A} \tag{1}$$

with deformation gradient $F_{\alpha\beta} = \partial x_\alpha / \partial X_\beta$, node A, material laws m being defined at A, elements e surrounding A and belonging to material m, and nodal volume $V_A = \sum_{m \in A} \sum_{e \in m} V_A^e$. V_A^e denotes the weight of node A arising in element e.

Most NI techniques can be expressed in this form. Instead of averaging discrete values, one may try to interprete nodally continuous strains in terms of a $C0$-continuous deformation gradient field which is defined in all material points. Since this field is not inherent to the given finite element interpolation, the field is called "assumed" in opposite to "natural". Let define it using Hu-Washizu type constraints, i.e.

$$0 = \delta\lambda_{A\alpha\beta} \int_V \left(M_A(\xi) N_B(\xi) F_{B\alpha\beta} - M_A(\xi) F_{\alpha\beta}(\xi) \right) dV \tag{2}$$

which weakly enforces the condition $F_{\alpha\beta}^{AN}(\xi) - F_{\alpha\beta}(\xi) \approx 0$. Herein, $F_{\alpha\beta}(\xi)$ denotes the deformation gradient derived from the finite element shape functions, $N_B(\xi) F_{B\alpha\beta}$ is the assumed field with support values at nodes B and interpolated using the finite element shape function N_B. The given discretized form is obtained by associating the constraint field with a Lagrange multiplier $\lambda_{\alpha\beta}(\xi) = M_A(\xi)\lambda_{A\alpha\beta}$ with support $\lambda_{A\alpha\beta}$ and interpolation function M_A.

Using the assumed field formulation, known NI methods differ in the choice of M_A and the numerical integration scheme $\int(\circ)dV$.

3 NODAL INTEGRATION AND LINEARIZATION

Let assume the existence of a strain energy potential function U and strain energy density U^d. Let interpolate the energy density using finite element shape functions such that

$$U = \int_V U^d(\epsilon, \alpha_{int}, t) dV = U_{\mathcal{A}}^m \int_{V^m} N_{\mathcal{A}}^m(\xi) dV \tag{3}$$

where the nodal values are evaluated at the finite element nodes by $U_{\mathcal{A}}^m = U^m(\epsilon^m(\mathbf{F}_{\mathcal{A}}), \alpha_{\mathcal{A}}^m, t)$ Herein, U^m denotes the constitutive relation defined for finite element group m, $\alpha_{\mathcal{A}}^m$ are the history variables at the considered material evaluation point. ϵ^m defines a function that computes the strain from the nodal deformation gradient $\mathbf{F}_{\mathcal{A}}$.

When solving the equation of motion, the strain energy is usually replaced by a quadratic expansion around the current configuration, i.e.

$$U(\mathbf{u} + \Delta\mathbf{u}, t) = U(\mathbf{u}, t) + \nabla U(\mathbf{u}, t)\Delta\mathbf{u} + \frac{1}{2}\Delta\mathbf{u}^T \nabla^2 U(\mathbf{u}, t)\Delta\mathbf{u} \tag{4}$$

In structural dynamics, the strain energy gradient ∇U is often called the restoring force $\mathbf{F}^{res}$ and the Hessian $\nabla^2 U$ is denoted as stiffness matrix $\mathbf{K}$. They are computed by

$$F_{\mathsf{A}} = \sum_m W_{\mathcal{B}}^m \sigma_{\mathcal{B}\alpha}^m \frac{\partial \epsilon_\alpha^m(\mathbf{F}_{\mathcal{B}})}{\partial F_{\mathcal{B}\beta\gamma}} \frac{\partial F_{\mathcal{B}\beta\gamma}}{\partial u_{\mathsf{A}}} \tag{5}$$

$$K_{\mathsf{AB}} = \sum_m W_{\mathcal{C}}^m \sigma_{\mathcal{C}\alpha}^m \frac{\partial^2 \epsilon_\alpha^m(\mathbf{F}_{\mathcal{C}})}{\partial F_{\mathcal{C}\beta\gamma} \partial F_{\mathcal{C}\eta\omega}} \frac{\partial F_{\mathcal{C}\beta\gamma}}{\partial u_{\mathsf{A}}} \frac{\partial F_{\mathcal{C}\eta\omega}}{\partial u_{\mathsf{B}}} + \tag{6}$$

$$\sum_m W_{\mathcal{C}}^m C_{\mathcal{C}\alpha\delta}^m \frac{\partial \epsilon_\alpha^m(\mathbf{F}_{\mathcal{C}})}{\partial F_{\mathcal{C}\beta\gamma}} \frac{\partial \epsilon_\delta^m(\mathbf{F}_{\mathcal{C}})}{\partial F_{\mathcal{C}\eta\omega}} \frac{\partial F_{\mathcal{C}\beta\gamma}}{\partial u_{\mathsf{A}}} \frac{\partial F_{\mathcal{C}\eta\omega}}{\partial u_{\mathsf{B}}} \tag{7}$$

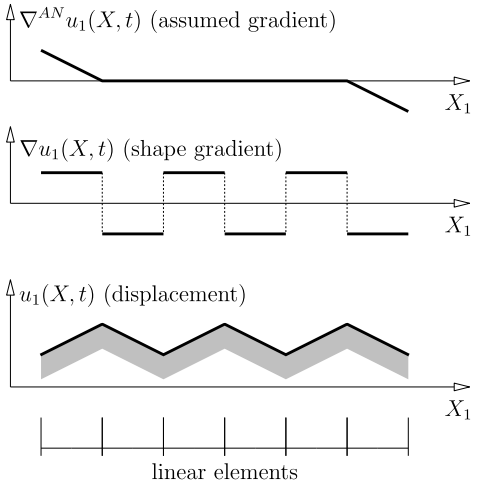

Figure 1: Failure of locally averaged deformation gradient in one dimension

wherein

$$\sigma^m_{\mathcal{A}\alpha} = \frac{\partial}{\partial \epsilon^m_\alpha} U^m_{\mathcal{A}}(\epsilon^m(\mathbf{F}_{\mathcal{A}}), \alpha^m_{\mathcal{A}}, t), \quad C^m_{\mathcal{A}\alpha\beta} = \frac{\partial^2}{\partial \epsilon^m_\alpha \partial \epsilon^m_\beta} U^m_{\mathcal{A}}(\epsilon^m(\mathbf{F}_{\mathcal{A}}), \alpha^m_{\mathcal{A}}, t) \tag{8}$$

denote the stress and tangential material tensor. $W^m_{\mathcal{A}}$ is an integration weight denoting the fictive volume of the m-th element group at material node $\mathcal{A}$, i.e. $W^m_{\mathcal{A}} = \int_{V^m} N^m_{\mathcal{A}}(\xi) dV$.

4 SPURIOUS MODES

Examples show that the presented strain smoothing operator does not invoke the appearance of spurious zero-energy modes. Unlike in reduced order integration, the kinematic relationship between the continuous deformation gradient and the natural shape function derivatives is established utilizing accurately evaluated integrals over the elemental volumes. Therefore, no rank deficiency occurs.

As being noted by several authors, NI leads to instabilities in terms of spurious low-energy modes. This defective may, however, not appear in many usecases. That is, whenever the respective mode shapes are not excited or when the mesh is fine such that local modes are not visible on the global level. The spurious modes become apparent when modal analyses is applied. Figure 7 shows a few examples of spurious eigen shapes. In order to reduce the degeneracies of the integration scheme, one can try applying a high order Gaussian integration rule by integrating the strain energy density at integration points in the element interior using the assumed strain field. Applying this scheme to 4-noded tetrahedral and 8-noded hexahedral elements leads to the same defectives as observed when using NI. On the other hand, if one applies NI utilizing the natural shape derivatives as strain measure (i.e. individual strains per node of each element), one may observe bad convergence in the sense that the smallest eigenvalues are overestimated, but no spurious modes appear. Therefore, one can refer the instabilities to the formulation of the assumed deformation gradient field.

The reason for the instability of NI is the inability of the assumed deformation gradient to capture certain deformation shapes. For example, consider a one dimensional domain with equally sized linear finite elements being deformed as shown in figure 1. The interior elements are highly deformed, but the nodal values of the continuous deformation gradient measure zero

strain. Only the nodal strain values that are located at the boundaries of the structure (where no averaging takes place) describe the strains exactly. Since the elements at the boundary induce a stiffness, the presented deformation shape is related to an eigenmode which energy is greater than zero, but greatly underestimated.

Therefore, the instabilities arise, because the continuous assumed deformation gradient losely satisfies

$$\int_V F_{\alpha\beta}^{AN} dV \approx \int_V \left(\nabla_\beta u_\alpha + \delta_{\alpha\beta}\right) dV \tag{9}$$

that expresses that the deformation gradient obtained from the shape function derivatives and the assumed deformation gradient are equal in the weak sense. But the assumed deformation gradient does not satisfy local equivalence, or, in other words, it does not minimize the local error in the element interior between the assumed field and the field obtained from the shape function derivatives. The latter can be expressed by a global error norm, i.e.

$$\int_V \left\| \nabla_\beta u_\alpha + \delta_{\alpha\beta} - F_{\alpha\beta}^{AN} \right\| dV \rightarrow \min \tag{10}$$

Solving equation (10) leads to equation (2) with $M_A(\xi) = N_A(\xi)$. Therefore, both conditions (9), (10) may be satisfied.

5 STABILIZATION

5.1 Consistent field approximation

With $M_A(\xi) = N_A(\xi)$, the nodal values $F_{B\alpha\beta}$ in (2) can be solved using the following approaches:

1. Lumping. One could invert the matrix $\int_V N_A N_B dV$ by assuming a lumping scheme

$$\int_V N_A(\xi) N_B(\xi) dV \rightarrow \delta_{AB} \int_V N_A(\xi) dV \tag{11}$$

   Therefore, the nodal values can be computed internally by $F_{A\alpha\beta}^{LM} = \frac{\int_V N_A(\xi) F_{\alpha\beta}(\xi) dV}{\int_V N_A(\xi) dV}$, see also equation (1). This solution leads to instabilities being discussed earlier.

2. The nodal values $F_{B\alpha\beta}$ can serve as additional degrees of freedom in order to extend the system of equation. Having n nodes would add $9n$ variables which is undesirable.

3. The nodal values $F_{B\alpha\beta}$ can be eliminated internally using full factorization. One can invert the matrix $\int_V N_A N_B dV$ previous to the simulation, since it is constant. An internal factorization is practically impossible, the inverse is dense. Therefore, the nodal values $F_{B\alpha\beta}$ would have a global support regarding the displacements $\mathbf{u}$.

This formulation is consistent and stable. It was exemplified using linear tetrahedral elements applying the third solution approach. The consistent formulation of the assumed deformation gradient is, however, only of theoretical importance, but can be used to understand existing and to develop new stabilization schemes. The most important properties of the formulation are that it weakly enforces (9) and minimizes the error between both fields in the elements' interior at the same time.

5.2 Penalty regularization

The error (10) can be reduced by application of the penalty method. Herein, the constraint (2) will be enforced approximately. This is done by creating a modified strain energy function U_{mod} through adding a penalizing potential function, such that $U_{mod}(\mathbf{u},t) = U(\mathbf{u},t) + P(\mathbf{u})$. P is chosen such that $U_{mod}(\mathbf{u},t) = U(\mathbf{u},t)$ if the constraint is satisfied and $P \gg 0$ if the constraint is violated. A possible choice is the quadratic penalty function

$$P(\mathbf{u}) = \rho \int_V \left\| F^{AN}_{\alpha\beta}(\xi) - F_{\alpha\beta}(\xi) \right\|^2 dV \tag{12}$$

with penalty parameter ρ which adjusts the allowed range of the constraint violation.

Since $\left\| F^{AN}_{\alpha\beta}(\xi) - F_{\alpha\beta}(\xi) \right\|$ may serve as a measure for the deviation of the discrete solution from exact solution, one may chose alternative constraints to be penalized. In [1] a penalty potential is presented that assumes that the strain energy is accurately evaluated at the nodes and an error in evaluating the potential appears in the element interior. This error is measured in terms of the strong (pointwise) stress residual, yielding

$$P_{Beissel}(\mathbf{u}) = \rho \int_V \left\| \frac{\partial U^d(\xi)}{\partial \mathbf{u}} - \mathbf{b}(\xi) \right\|^2 dV \tag{13}$$

wherein $\mathbf{b}$ denotes the vector of applied body forces. In order to provide a simple expression for the variations of P, the constitutive law is replaced by a linear elastic material. The scaling parameter is determined from $\rho = \frac{\alpha l_c}{E}$ with parameter α, characteristic length l_c and elastic modulus E. In [10], a penalty of the form

$$P_{Broccardo}(\mathbf{u}) = \rho \int_V \mathrm{tr}\left[\left(\mathbf{F}^{AN} - \mathbf{F} \right)^T \left(\mathbf{F}^{AN} - \mathbf{F} \right) \right] dV \tag{14}$$

was implemented.

5.3 Conforming regularization

In [9], a stabilization is presented which develops the ideas shown in [1]. The question is if it is possible to add a penalty potential function, such that the strain energy function behaves like a Gaussian integrated finite element energy in the limit of infinitesemal strains. Furthermore, the stability and linear exactness could be provided by the stabilization term; material nonlinearities are subject to the nodally integrated parts. The basic idea is to understand the nodal deformation gradient as a strain measure which is not conform with the shape function space of the displacements. Then one modifies the strain energy such that

$$U_P(\mathbf{u},t) = U(\mathbf{u},t) - U^{C1}(\mathbf{u}) + U^{C0}(\mathbf{u}) \tag{15}$$

Therein, $U(\mathbf{u},t)$ denotes the nodally integrated strain energy. $U^{C1}(\mathbf{u})$ represents a nodally integrated strain energy potential which approximates $\mathbf{U}(u,t)$ using the continuous deformation gradient. $U^{C0}(\mathbf{u})$ denotes a conformingly integrated strain energy potential which approximates $\mathbf{U}(u,t)$ using the finite element shape function derivatives. Then

$$U_P(\mathbf{u},t) \approx U^{C0}(\mathbf{u}), \quad \text{if} \quad \epsilon(\xi) \approx \mathbf{0} \tag{16}$$

which does not exhibit any instabilities. For the two additional energy functions a linear elastic material is used in order to provide efficient linearizations, such that the material tensor $\mathbf{C}^s$ of the stabilizing strain energy density

$$U^s(\xi,\epsilon)C^s_{\alpha\beta\gamma\delta}(\xi) = \left.\frac{\partial^2 U^d(\xi,\epsilon,t)}{\partial\epsilon_{\alpha\beta}\partial\epsilon_{\gamma\delta}}\right|_{\epsilon=0,\,t=0} \tag{17}$$

In the case of incompressible media this setting would degrade the resistance of nodal integration against volumetric locking. Therefore, the Possion ratio is decreased in the stabilizing potential such that $\max(\nu) = 0.3$. In the case of nonlinear material laws a material tensor representing the characteristic behaviour is recommended in favour of the initial tangent material stiffness.

Let derive a special form in case of infinitesemal strains. The nodally averaged deformation gradient is reexpressed for convenience, $F_{A\alpha\beta} = \frac{1}{V_A}\sum_{e\in A} V_e F_e$ where F_e denotes the deformation gradient at node A obtained from the finite element shape functions at element e; V_A is the nodal volume being the sum of the contributions of the surrounding elements e, i.e. $V_A = \sum_{e\in A} V_e$. The second variation of the strain energy yields

$$\delta^2 U_P = \sum_A V_A \left(\delta\mathbf{F}_A^T \frac{\partial^2 U_A^d}{\partial\mathbf{F}\partial\mathbf{F}}\delta\mathbf{F}_A - \delta\mathbf{F}_A^T \frac{\partial^2 U_A^s}{\partial\mathbf{F}\partial\mathbf{F}}\delta\mathbf{F}_A + \sum_{e\in A}\frac{V_e}{V_A}\delta\mathbf{F}_e^T \frac{\partial^2 U_A^s}{\partial\mathbf{F}\partial\mathbf{F}}\delta\mathbf{F}_e \right) \tag{18}$$

With (16) this can also be expressed as

$$\begin{aligned}
\delta^2 U_P &= \delta^2 U^{C0} = \sum_A \sum_{e\in A} V_e \left(\delta\mathbf{F}_e^T \frac{\partial^2 U_A}{\partial\mathbf{F}\partial\mathbf{F}}\delta\mathbf{F}_e \right) && (19)\\
&= \sum_A \left[\sum_{e\in A} V_e \delta\mathbf{F}_e^T \frac{\partial^2 U_A}{\partial\mathbf{F}\partial\mathbf{F}}\delta\mathbf{F}_e + V_A \left(\delta\mathbf{F}_A^T \frac{\partial^2 U_A}{\partial\mathbf{F}\partial\mathbf{F}}\delta\mathbf{F}_A - \delta\mathbf{F}_A^T \frac{\partial^2 U_A}{\partial\mathbf{F}\partial\mathbf{F}}\delta\mathbf{F}_A \right) \right] && (20)\\
&= \sum_A \left[V_A \left(\delta\mathbf{F}_A^T \frac{\partial^2 U_A}{\partial\mathbf{F}\partial\mathbf{F}}\delta\mathbf{F}_A \right) + \sum_{e\in A} V_e \left(\delta\mathbf{F}_A^T - \delta\mathbf{F}_e^T \right) \frac{\partial^2 U_A}{\partial\mathbf{F}\partial\mathbf{F}} \left(\delta\mathbf{F}_A - \delta\mathbf{F}_e \right) \right] && (21)\\
&= \delta^2 U + \delta^2 \int_V \left(\left\| \mathbf{F}^{AN} - \mathbf{F} \right\|^2_{\frac{\partial^2 U^s}{\partial\mathbf{F}\partial\mathbf{F}}} \right) dV && (22)
\end{aligned}$$

Therefore, the conformization can be interpreted in terms of a quadratic penalty term, where the norm of the constraint residual is weighted by a material tensor. It can be combined with a penalty parameter α which may have values between 0 (not stabilized) and 1 (full stabilized). If the infinitesemal strain tensor is used, then the stabilizing stiffness $\mathbf{K}^s = \alpha\nabla^2_{\mathbf{u}}\left(U^{C0} - U^{C1}\right)$ is constant and can be precomputed previous to the simulation yielding an efficient scheme. It is possible to extend the idea to the case of geometrically nonlinear strains, yielding $U^\alpha_P(\mathbf{u},t) = U(\mathbf{u},t) + \alpha\left(U^{C0}(\mathbf{u}) - U^{C1}(\mathbf{u})\right)$

The presented conforming regularization is a promising approach since it stabilizes nodal integration and formulates an artificial energy which is close to the physical model. As any regularization method it exhibits a few limitations, these are

- It adds artificial energy which may become quite large even for relative fine meshes. The artificial energy is a measure of discretization error. It can be reduced by finer remeshing and by decreasing the penalty parameter. The penalty parameter is chosen to be at least

large enough to increase the eigenvalue of the spurious modes such that their degree of excitation is negligable. Therefore, the optimal choice of the penalty parameter may be dependent on the mesh topology and loading.

- When applied to nonlinear strain measures, the numerical effort increases by a factor three, since three nonlinear strain energy functions must be evaluated at each node.

- Since the stabilizing energy density is evaluated at the same spatial coordinate as the strain energy density of the given material, both contribute to the modified stress distribution $\sigma_P(\xi) = \sigma(\xi) + \sigma^s(\xi)$ Therefore, the stress arising from the nodally evaluated strain energy density σ is smaller compared with unstabilized integration. When nonlinear effects (plastic strains, failure and yield conditions) are of interest, their magnitude is systematically underestimated.

6 STABILIZATION BY MIXED INTEGRATION

6.1 Dual Lagrange multiplier field

For the special case of finite element shape functions of tensor-product structure, a certain choice for M_A in equation (2) leads to a lumped matrix structure of the discrete constraint gradients, and, thus, the nodal multipliers can be eliminated internally. Assume that the so called dual multiplier space, see [12], is constructed by the linear combination

$$M_A(\xi) = a_{AB} N_B(\xi) \tag{23}$$

where a_{AB} denotes some coefficient matrix. One can consider each element separately. Then, the dual shape functions are individually defined for each finite element and the local coefficients a_{ij} are not equal for neighboring elements in general. Since the dual shape is defined by a linear combination of the original shape function space, it inherits most of the properties, for example C^0continuity. Since the coefficients a_{ij} are computed for each element, all volume integrations are restricted to the domain of a single finite element. In order to obtain a lumped matrix scheme, the biorthogonality criterion

$$\int_V M_A(\xi) N_B(\xi) dV = \delta_{AB} \int_V N_A(\xi) dV \tag{24}$$

must be satisfied, written by splitting the integration domain into finite elements

$$\sum_e \int_{V^e} M_{\text{node}(e,i)}(\xi) N_{\text{node}(e,j)}(\xi) dV = \sum_e \delta_{ij} \int_{V^e} N_{\text{node}(e,i)}(\xi) dV \tag{25}$$

Using the definitions $n_{ij} = \text{diag}(\int_{V^e} N_i(\xi) dV)$ denoting the target diagonal matrix, $m_{ij} = \int_{V^e} N_i(\xi) N_j(\xi) dV$ denoting a symmetric matrix, one obtains

$$\int_{V^e} M_i(\xi) N_j(\xi) dV = a_{ik} \int_{V^e} N_k(\xi) N_j(\xi) dV \tag{26}$$

$$n_{ij} = a_{ik} m_{kj} \tag{27}$$

$$a_{ik} = n_{ij} m_{jk}^{-T} = m_{kj}^{-1} n_{ij} \tag{28}$$

If dual multiplier spaces are applicable, the discrete constraint yields

$$0 = \delta_{AB} \int_V N_B(\xi) F_{B\alpha\beta} dV - \int_V M_A(\xi) F_{\alpha\beta}(\xi) dV$$

Using the notations

$$\begin{aligned} \int_V N_B(\xi) F_{B\alpha\beta} dV &= V_B F_{B\alpha\beta} \\ F_{\alpha\beta}(\xi) &= N_C(\xi) F^e_C \; \forall e, \, \xi \in e \end{aligned}$$

one obtains

$$F_{A\alpha\beta} = \frac{\int_V M_A(\xi) \nabla_\gamma N_B(\xi) J^{-1}_{\gamma\beta}(\xi) dV}{\int_V N_A(\xi) dV} u_{B\alpha} + \delta_{\alpha\beta} = \frac{1}{V_A} \sum_{m \in A} \sum_{e \in A} V^e_A F^e_{A\alpha\beta} \tag{29}$$

The nodal deformation gradient $F_{A\alpha\beta}$ has compact support, i.e. it depends on the degrees of freedom of all finite elements adjacent to node A. Obviously, using linear tetrahedral shape functions, this formulation is identical with [5, 7].

In special cases ($\det(J)$ =const. within a single element) the support is sparse, i.e. only a few nodes of the adjacent elements contribute to the deformation gradient.

Though no approximating assumptions were made, the dual formulation still leads to spurious modes. In opposite to alternative averaging methods, it has the important ability to describe hourglass deformation shapes.

6.2 Mixed integration

Let derive a penalty regularization which does not add any artificial energy to the system. Start with the observation that the nodal values of the deformation gradient are well approximated (if the finite elements would be C^1-continuous), but not the values in the element interior. Therefore, select an integration rule which requires integration points in the nodes A and in the element interior i leading to the penalized potential

$$U = \sum_A \sum_{m \in A} W_m U^m(\mathbf{F}_A) + \sum_i W_i U^i \left(\mathbf{F}^{AN}(\xi_i) \right) + \alpha \sum_i W_i U^s \left(\mathbf{F}(\xi_i) - \mathbf{F}^{AN}(\xi_i) \right) \tag{30}$$

Therein, m represents different materials defined at node A, W_m denote the associated integration point volumes and $\mathbf{F}^{AN}(\xi_i)$ is the interpolated assumed deformation gradient at the i-th integration point. Since the deficiency of the assumed deformation gradient can be expected in the element interior, a penalty potential is evaluated only at the interior integration points,

$$\int_V \left(\left\| \mathbf{F} - \mathbf{F}^{AN} \right\|^2_{\frac{\partial^2 U^s}{\partial \mathbf{F} \partial \mathbf{F}}} \right) dV \approx \sum_i W_i U^s \left(\mathbf{F}(\xi_i) - \mathbf{F}^{AN}(\xi_i) \right)$$

whereby the error norm is weighted by a material tensor. Subsequently, the penalized strain energy will be replaced by a similar expression, which is identical for linear elastic materials and small strains, i.e.

$$U = \sum_A \sum_{m \in A} W_m U^m(\mathbf{F}_A) + \sum_i W_i U^i \left(\mathbf{F}(\xi_i) \right)$$

	nodal integration	reduced quadrature[3]	mixed integration
rigid body modes	good	good	good
constant strain modes	good	good	good
shear modes	bad	good	good
hourglass modes	good[1],bad[2]	failure	good[1],bad[2]

Table 1: Limitations of mixed integration schemes
[1] in case of exact formulation utilizing dual Lagrange multiplier spaces
[2] in case of inexact formulation utilizing lumping assumption, or in case of piecewise constant multiplier space
[3] linear tetrahedron (4n) and hexahedron (8n): 1 point, quadratic tetrahedron (10n): 4 points, quadratic hexahedron (27n): 8 points

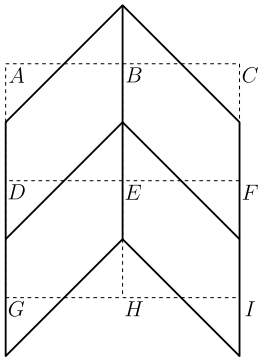

Figure 2: Shear deformation shape

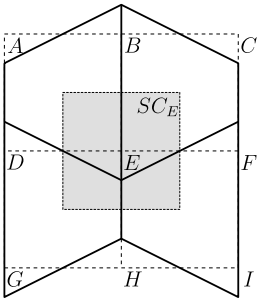

Figure 3: Hourglass deformation shape

This scheme stabilizes nodal integration depending on the properties of the innerelemental integration scheme. One possible choice is to adopt full Gaussian integration for the element interior. For linear hexahedral and tetrahedral elements it is sufficient to add a single integration point in the element center. By doing so one literally combines nodal integration and reduced Gaussian integration in order to eliminate the limitations of both individual schemes, see table 6.2. The integration weights $W_{\mathcal{A}}$ can be computed by interpreting the associated points as supporting points of a polynomial shape function $N_{\mathcal{A}}$ of a finite element with additional nodes in the element interior.

Let analyze the mixed integration scheme a little deeper. The one-point Gaussian integration for 8-noded hexahedrals leads to zero-energy modes because it evaluates the deformation gradient at those points where the hourglass mode shapes lead to zero strains. The integration scheme is numerically exact, if integration points are added at special locations, notibly where hourglass mode shapes are accurately measured. On the other hand, the nodal values of the deformation gradient will be computed such that interior nodal values measure zero strain if certain mode shapes are applied. Since the interpolation of the assumed field depends on the nodal support points, the deformation gradient will be erroneously measured in all adjacent elements, independent of the integration scheme. Only a different interpolation scheme of the deformation gradient could solve the issue. Such a scheme is given by measuring the natural gradients in the element interior. When combining both methods, then it must be assured that all mode shapes which are falsely measured by the one method are correctly covered by the other.

Consider, for example, the application of shear deformation shapes onto a structure as shown in figure 2. Obviously, an average of the deformation gradients at node E is the identity matrix.

When imposing hourglass deformation shapes the interpolation quality depends on the averaging operator, see figure 3. A plain average of the deformation gradients at node E and the integrated average over the smoothing cell SC_E measure zero strain. In the case of continuous Lagrange multipliers, the averaged deformation gradient is an integrated average which is weighted by the multiplier shape function of node E. Therefore, the hourglass modes lead to nonzero strains when using dual multiplier spaces. If standard multiplier spaces are applied and approximately solved assuming lumping quantities, numerical experiments show that the simplification leads to similar instabilities as constant multipliers. In order to continue the analysis, one has to analyze all 18 mode shapes of the illustrated two-dimensional structure and check, in which deformation shapes are correctly displayed by the assumed deformation field.

As a result, nodal integration using dual multiplier spaces for the construction of an assumed deformation gradient field and reduced Gaussian integration complement each other when imposing shear and hourglass deformation shapes. Rigid body motions and constant strain deformation shapes are well represented by both schemes. Therefore, a mixed integration of both leads to a stable scheme.

6.3 Computing integration point weights

An integral

$$I = \int_V f(\mathbf{X}) dV$$

is evaluated numerically by the sum

$$I = \sum_{\mathcal{A}} W_{\mathcal{A}} f(\mathbf{X}_{\mathcal{A}})$$

with integration weight $W_{\mathcal{A}}$ which can be interpreted in terms of a nodal volume, that is the volume surrounding integration point $\mathcal{A}$. In terms of nodal integration, the integration points are the FEM nodes A and the innerelemental integration points i from mixed integration. In order to compute the nodal volumes, one may chose a polynomial interpolation $f^h(\mathbf{X})$ approximating $f(\mathbf{X})$. Then,

$$I = \int_V f^h(\mathbf{X}) dV = \int_V \sum_{\mathcal{A}} N_{\mathcal{A}} f(\mathbf{X}_{\mathcal{A}}) dV$$

and

$$W_{\mathcal{A}} = \int_V N_{\mathcal{A}} dV$$

In the case of nodal integration, the shape functions $N_{\mathcal{A}}$ are the finite element shape functions. If a mixed integration scheme is chosen, then $N_{\mathcal{A}}$ are the shape functions of a finite element with additional interior nodes. Table 2 lists the shape functions for a few finite element types. For the elements C3D_4N and C3D_8N an additional node in the element center is added and associated with a bubble shape function.

7 EXAMPLE

7.1 Patch test

The patch test verifies the ability to represent constant strain fields. To do so, a linear deformation field ist applied to a structure with irregular element geometries. In figure 4 a structure

C3D_4N	C3D_5N
$N_1^4(\xi) = 1 - \xi_1 - \xi_2 - \xi_3$ $N_2^4(\xi) = \xi_1$ $N_3^4(\xi) = \xi_2$ $N_4^4(\xi) = \xi_3$	$N_i^5(\xi) = N_i^4(\xi) - \frac{1}{4}N_5^5(\xi)\ \forall i = 1 \dots 4$ $N_5^5(\xi) = 256\xi_1\xi_2\xi_3(1 - \xi_1 - \xi_2 - \xi_3)$
C3D_8N	**C3D_9N**
$N_1^8(\xi) = \frac{1}{8}(1 + \xi_1)(1 + \xi_2)(1 + \xi_3)$ $N_2^8(\xi) = \frac{1}{8}(1 - \xi_1)(1 + \xi_2)(1 + \xi_3)$ $N_3^8(\xi) = \frac{1}{8}(1 - \xi_1)(1 - \xi_2)(1 + \xi_3)$ $N_4^8(\xi) = \frac{1}{8}(1 + \xi_1)(1 - \xi_2)(1 + \xi_3)$ $N_5^8(\xi) = \frac{1}{8}(1 + \xi_1)(1 + \xi_2)(1 - \xi_3)$ $N_6^8(\xi) = \frac{1}{8}(1 - \xi_1)(1 + \xi_2)(1 - \xi_3)$ $N_7^8(\xi) = \frac{1}{8}(1 - \xi_1)(1 - \xi_2)(1 - \xi_3)$ $N_8^8(\xi) = \frac{1}{8}(1 + \xi_1)(1 - \xi_2)(1 - \xi_3)$	$N_i^9(\xi) = N_i^8(\xi) - \frac{1}{8}N_9^9(\xi)\ \forall i = 1 \dots 8$ $N_9^9(\xi) = (1 - \xi_1^2)(1 - \xi_2^2)(1 - \xi_3^2)$

Table 2: Finite element shape functions for nodal integration and bubble shape functions for mixed integration

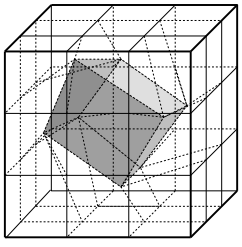

Figure 4: Patch test

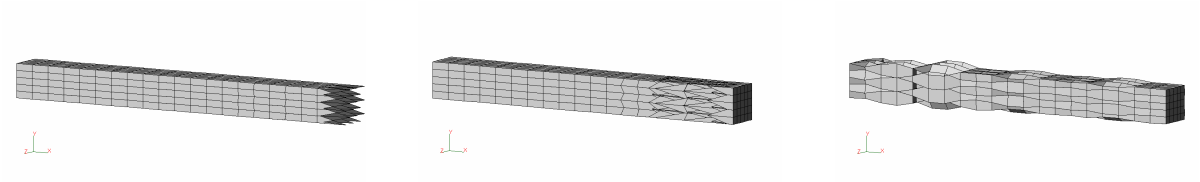

Figure 5: Eigenmodes for nodally integrated simple averaging operator of a cantilever beam (2 zero energy modes and the 45th smallest mode)

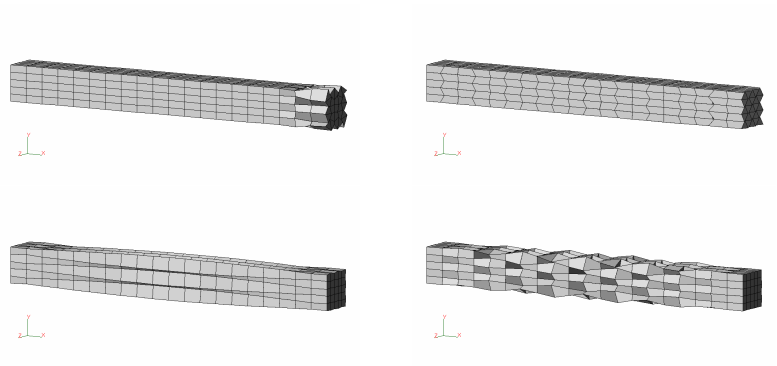

Figure 6: Eigenmodes for mixed integrated simple averaging operator of a cantilever beam (the 1st, 14th, 19th and 21th eigenshapes)

consisting of $3 \times 3 \times 3$ 8-noded brick elements is shown, where the nodal coordinates of the center element are randomly chosen. Application of a displacement field given through the nodal displacements

$$u_{A\alpha} = u_{0\alpha} + a_\alpha X_{A\alpha}$$

and measurement of the deformation gradients at all integration points proves the patch test. The test may be expanded to other element types by inserting additional nodes (for example for C3D_27N elements) or subdividing the hexahedrals into tetrahedral elements.

7.2 Modal analysis of a cantilever beam

Consider a cantilever beam of dimensions $1m \times 0.1m \times 0.1m$ made of steel with elastic modulus $E = 2.06 \cdot 10^9 N/m^2$, Poission number $\nu = 0$ and mass density $E = 7.85 \cdot 10^6 g/m^3$. The beam is clamped on its left side. The structure is discretized by $5 \times 5 \times 20$ 8-noded hexahedral elements.

The instabilities can be well observed using modal analyses. Consider nodal integration as presented in [8]. Figure 5 presents a few mode shapes of the structure. The first two are classical hourglass modes being associated with zero eigenvalues. The third is a spurious mode which combines shear and hourglass modes being associated to a spurious low-energy mode (the 45th smallest eigenvalue). Therefore, a stabilization by mixed integration with a reduced order scheme is not possible, as illustrated in figure 6. The figure shows the 1st, 14th, 19th and 21th spurious eigenmode shapes. In all of them the hourglass deformation is dominant. Only the portions of shear and constant strain provide some terms to the associated small eigenvalues.

A further improvement is provided by the assumed gradient operator with lumping assumption given by (11). The zero-energy modes are eliminated. Still, spurious low-energy modes appear as illustrated in figure 7. Herein, the 10th and 14th eigenshapes are presented where

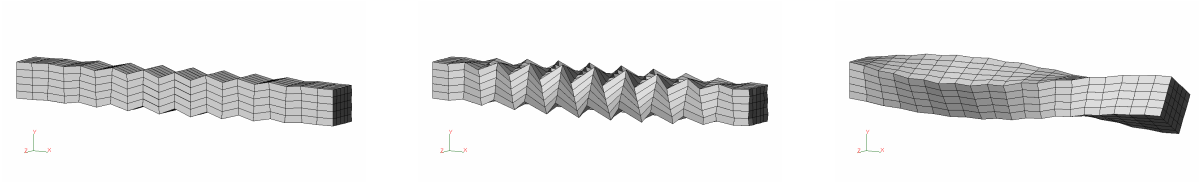

Figure 7: Eigenmodes for nodally integrated lumped averaging operator of a cantilever beam (the 6th, 16th, and 14th eigenshapes)

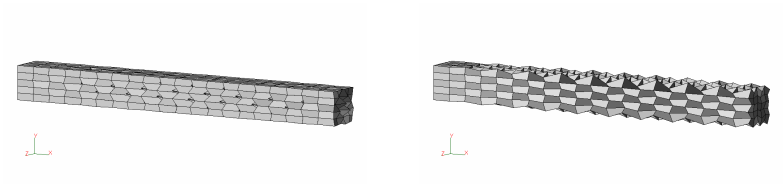

Figure 8: Eigenmodes for mixed integrated lumped averaging operator of a cantilever beam (the 41th and 50th eigenshapes)

either shear or hourglass deformations are dominant. The subsequent modes, for example the presented bending (mode 13), also contain nonphysical components. Using mixed integration, situation improves considerably. The first non-physical mode appears at position 41. Figure 8 illustrates the 41th and 50th eigenmode shapes wherein hourglassing is dominant.

Using dual multiplier spaces to derive a compact assumed gradient operator, see equation (29), is very similar. Figure 9 illustrates the spurious 6th and 11th eigenmode shapes and the 14th (physical) eigen mode shape which is greatly distorted by previous nonphysical modes. Compared with the lumped operator, the spurious mode shapes contain dominant shear deformations, but not hourglass effects. When applied to mixed integration, no non-physical modeshapes were observed when computing the smallest 500 eigenvalues.

When using 4-noded tetrahedrals, the solution of the presented averaging operators is equal. In all cases, mixed integration stabilizes the method. When using 10-noded tetrahedrals, nodal integration in combination with 4-point Gauss integration is stable, when using 27-noded hexahedrals utilizing 8-point Gauss integration.

7.3 Convergence of eigenvalues

Table 7.3 lists the three smallest eigenvalues of the cantilever beam for different configurations. The cases differ in the used meshing (number of elements per side) and the used finite element types, i.e. classical eight noded hexahedron C3D_8N, nodally (mixed) integrated hexahedron C3D_8N_NI, classical four noded tetrahedron C3D_4N and nodally (mixed) integrated tetrahedron C3D_4N_NI.

Obviously, the continuous strain field reduces the overestimation of the stiffness in case of

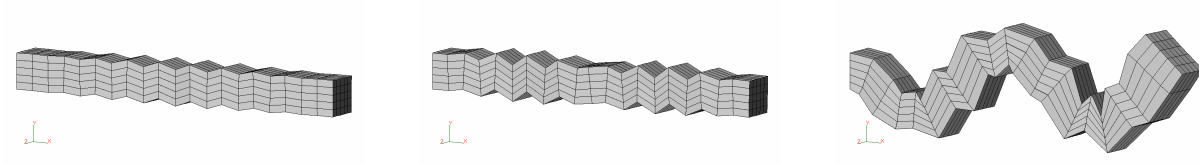

Figure 9: Eigenmodes for nodal integrated dual averaging operator of a cantilever beam (the 6th, 11th and 14th eigenshapes)

mesh	c3d_8n	c3d_8n_NI	c3d_4n	c3d_4n_NI
$3 \times 3 \times 3$	17.2210	8.9259	40.2780	17.0750
	17.2210	8.9259	61.7400	24.9680
	310.0500	327.61	662.1800	622.0600
$5 \times 3 \times 3$	7.9502	4.2620	16.9810	7.4840
	7.9502	4.2620	27.0630	10.8470
	303.2500	157.1900	585.1200	270.2100
$10 \times 3 \times 3$	4.0351	3.1887	6.6800	3.7432
	4.0351	3.1887	9.4850	4.5899
	150.1400	112.1700	239.7100	134.5500
$20 \times 3 \times 3$	3.0333	3.0461	4.0986	2.8493
	3.0333	3.0461	4.8193	3.0180
	110.7100	108.6700	148.5000	103.06000
$20 \times 5 \times 5$	3.0894	2.7808	3.6912	2.8966
	3.0894	2.7808	4.8928	3.0450
	110.4800	101.3900	136.3000	105.2400
$20 \times 7 \times 7$	2.8715	2.8578	3.7337	2.8974
	2.8715	2.8578	4.7164	3.1034
	110.1900	99.5620	133.0100	106.0900
$30 \times 15 \times 15$	3.5462	2.0164	2.1888	2.9153
	3.5462	2.0164	5.0693	3.0093
	103.7600	96.9950	113.6200	101.7200

Table 3: Convergence of smallest three eigenvalues for different meshes

rough meshes. Further experiments may also show its resistence against volumetric locking using incompressible materials. Compared with Gaussian integrated elements, the eigenvalues are better approximated regarding the mesh density. For example, it is well known that the linear tetrahedron exhibits very poor convergence, though its nodally integrated pendant approaches the convergence properties of the linear hexahedron. In general, one may losely find the ordering

$$\text{C3D\_4N} < \text{C3D\_4N\_NI} \approx \text{C3D\_8N} < \text{C3D\_8N\_NI}$$

There is one open issue to be discussed, that is the accuracy of the approximated eigenvalues. When applying NI to fine meshes the first pure bending modes are little underestimated.

Let consider numerical efficiency. Comparing the mesh resolution $10 \times 3 \times 3$, C3D_4N requires 450 integration points (a simple hexahedron may be decomposed into 5 tetrahedrons), C3D_4N_NI 626, C3D_8N 720 and C3D_8N_NI only 266.

8 CONCLUSIONS

In this paper, nodal integration was briefly reviewed. The procedure of averaging the strains at the nodes was replaced by a continuous assumed natural field of the deformation gradient in terms of a geometric constraint. Existing stabilization techniques were interpreted and reexpressed in a penalty regularized form of this constraint. The limitations of the consistent solution were discussed. Therefore, an alternative stabilization method was developed. The latter appears to be computationally efficient and accurate. In fact, compared with other (also reduced) integration techniques it exhibits oustanding numerical performance, very well approximation of deformation shapes and good convergence behaviour.

The development of the presented approach continues by extending it to higher order finite elements.
[1]

REFERENCES

[1] Stephen Beissel and Ted Belytschko. Nodal integration of the element-free galerkin method. *Computer Methods in Applied Mechanics and Engineering*, 139(1-4):49 – 74, 1996.

[2] J. Bonet and A.J. Burton. A simple average nodal pressure tetrahedral element for incompressible and nearly incompressible dynamic explicit applications. *Communications in Numerical Methods in Engineering*, 14:437–449, 1998.

[3] J. Jung S. W. Key C.R. Dohrmann, M. W. Heinstein and W. R. Witkowski. Node-based uniform strain elements for three-node triangular and four-node tetrahedral meshes. *International Journal for Numerical Methods in Engineering*, 47(9):1549–1568, 2000.

[4] K. Miller G. R. Joldes, A. Wittek. Improved linear tetrahedral element for surgical simulation. *Proceedings of MICCAI Workshop*, pages 54–66, Oct. 2006.

[5] H. Marriott J. Bonet and O. Hassan. An averaged nodal deformation gradient linear tetrahedral element for large strain explicit dynamic applications. *Communications in Numerical Methods in Engineering*, 17(8):551–561, 2001.

[6] P. Krysl and B. Zhu. Locking-free continuum displacement finite elements with nodal integration. *International Journal for Numerical Methods in Engineering*, 2008.

[7] Liu, G., Dai, K., Nguyen, and T. A smoothed finite element method for mechanics problems. *Computational Mechanics*, 39(6):859–877, May 2007.

[8] G. R. Liu, T. Nguyen-Thoi, H. Nguyen-Xuan, and K. Y. Lam. A node-based smoothed finite element method (ns-fem) for upper bound solutions to solid mechanics problems. *Comput. Struct.*, 87(1-2):14–26, 2009.

[9] E. Zywicz M. A. Puso, J. S. Chen and W. Elmer. Meshfree and finite element nodal integration methods. *International Journal for Numerical Methods in Engineering*, 74(3):416–446, 2008.

[10] M. Micheloni M. Broccardo and P. Krysl. Assumed-deformation gradient finite elements with nodal integration for nearly incompressible large deformation analysis. *International Journal for Numerical Methods in Engineering*, 2008.

[11] M. A. Puso and J. Solberg. A stabilized nodally integrated tetrahedral. *International Journal for Numerical Methods in Engineering*, 67(6):841–867, 2006.

[12] Barbara I. Wohlmuth. A mortar finite element method using dual spaces for the lagrange multiplier. *SIAM J. Numer. Anal*, 38:989–1012, 1998.

[1] The research was funded by the FWF (Austrian Science Fund).